Trans Indian Inst Met (2020) 73(3):821–830
https://doi.org/10.1007/s12666-020-01892-1

ORIGINAL ARTICLE

Phase Evolution and Thermal Stability of Mechanically Alloyed AlCrFeCoNiZn High-Entropy Alloy

Vikas Shivam[1] · Vadapalli Sanjana[1] · N. K. Mukhopadhyay[1]

Received: 13 November 2019 / Accepted: 29 January 2020 / Published online: 24 February 2020

Abstract In the present investigation, a newly designed composition of equiatomic AlCrFeCoNiZn high-entropy alloy (HEA) has been synthesized by mechanical alloying. The milled powder after 30 h exhibited the formation of a single solid solution phase of BCC crystal structure with lattice parameter, $a = 2.87 \pm 0.02$ Å. Decomposition of the single-phase BCC structure into the two-phase, tetragonal (Cr–Co)-based σ phase ($a = 8.81$ Å, $c = 4.56$ Å)- and $L1_2$ ($a = 3.59 \pm 0.02$ Å)-type intermetallics was observed at temperature of ~ 800 °C (1073 K). However, after heat treatment of the 30 h milled powder at the temperatures of 300 °C (573 K) and 600 °C (873 K), similar type of phases was also noticed to coexist along with B2 ($a = 2.87 \pm 0.03$ Å)-type phase. This behaviour of the alloy confirms the diffusive nature of the phase transformation. The consolidated bulk alloy exhibited similar type of phases after sintering at 950 °C (1223 K).

Keywords Mechanical alloying (MA) · High-entropy alloy · In situ X-ray diffraction · Thermal stability

1 Introduction

The concept of the high-entropy alloys (HEAs) has been recently advocated and it has led to intense excitement among the materials research community. Earlier, the design of alloy was based on one or two principal alloying elements and other alloying elements were added in minor proportions to enhance the desired properties [1]. The alloy designs were mainly governed by the Hume–Rothery rules proposed for the binary alloys to form a substitutional solid solution. The hypothesis for multicomponent alloys that may form intermetallic compounds has been revised by the pioneering work of Yeh et al. [2] and Cantor et al. [3]. Both the groups have worked separately and established the evolution of the disordered solid solution phases in multi-component alloys opening up the new avenue of alloy design [4]. High-entropy alloys (HEAs) are usually defined as the alloys consisting of five or more principal alloying elements in the range of 5–35 at% for the equiatomic or non-equiatomic composition and possessing configuration entropy above 1.6 R (where R is the universal gas constant) [5, 6]. Earlier, it has been thought that high mixing entropy of these alloys prevents them from forming intermetallic compounds and consists mainly of solid solutions (crystalline or amorphous) [7–9]. However, there is also the possibility of the formation of intermetallic compounds and amorphous phases [10–12].

High-entropy alloys are developed by different processing routes, i.e. vacuum arc melting, vacuum induction melting, melt spinning, rapid solidification, vapour deposition technique and solid-state techniques [13–16]. However, most of the HEAs are produced by melting routes [17]. The common problem of the conventional melting route is the non-homogeneous microstructure in the solidified product. Therefore, it is essential to do the annealing at higher temperature followed by quenching to obtain the homogeneous structure. From the literature, it is estimated that only about 5% of high-entropy alloys have been developed by the solid-state technique of mechanical alloying (MA) [18]. Murty et al. [19] prepared the nanostructured solid solution of high-entropy alloys by

✉ Vikas Shivam
vikas.rs.met13@itbhu.ac.in

[1] Department of Metallurgical Engineering, Indian Institute of Technology (BHU), Varanasi 221005, India

mechanical alloying. Through MA, almost any kind of homogeneous material can be produced at room temperature avoiding segregation and inhomogeneous microstructure [20–22]. The concern of consolidation has been addressed to some extent by using advanced sintering technique, i.e. hot isostatic pressing (HIP), vacuum hot pressing (VHP) and spark plasma sintering (SPS). Varalakshmi et al. [23] reported the systematic study of AlTiCoNiCuZn high-entropy alloy by MA and discussed on how the phases evolved after the addition of elements in a binary CuNi alloy. Vaidya et al. [24] have come up with a new approach to design high-entropy alloy by sequential milling and reported how the phase fraction of evolving phases was changed by the choice of the initial binary composition. In our previous work, we have reported AlCrFeCoNi and AlCrMnFeCoNi high-entropy alloy produced by mechanical alloying and studied the dissolution of the elements with milling time [25, 26]. In both the alloys, a single-phase BCC structure was obtained with good chemical homogeneity and better thermal stability.

High-entropy alloys are getting more attention due to their promising properties which include high hardness, strength, excellent wear resistance, high corrosion resistance and good thermal stability due to their multiphase microstructure [27, 28]. Their metastable phases may change and lead to a new structure when subjected to heat treatments. The formation of the secondary phases has been reported in the literature. It has been found that the evolution of the new phases after the heat treatment is mainly dependent on the alloy composition, processing routes, initial phases and heat treatment process. Praveen et al. [29] have found that after spark plasma sintering (SPS) at 900 °C for AlCrFeCoCu HEA, the major BCC phase transformed into the ordered BCC phase. In the same study of phase evolution, they have reported the formation of σ phase in all the Cr-containing alloys.

The aim of the present investigation is to understand the alloying behaviour and thermal stability of the AlCrFeCoNiZn high-entropy alloy. To the best of our understanding, AlCrFeCoNiZn high-entropy alloy has not yet been investigated by any processing route. The evolution of phases, microstructure and thermal stability has been investigated. Attempts have been made to discuss some aspects of forming ability and stability of the present high-entropy alloy.

2 Experimental Procedure

Elemental powders of Al, Cr, Fe, Co, Ni and Zn of purity ≥ 99% were taken as the starting material. These elemental powders were mixed in the equiatomic (16.66%) composition and milled in the high-energy planetary ball mill (Retsch PM 400) with the rotation speed of vials at 200 rpm. Milling was done in the wet atmosphere of toluene with the ball-to-powder weight ratio of 10:1 in tungsten carbide (WC) vials. In order to understand the milling behaviour, the powder was extracted at a regular interval of time for X-ray diffraction experiment. For X-ray diffraction analysis, Rigaku MiniFlex 600 (40 kV, 15 mA) with Cu $K\alpha$ radiation was used. The pseudo-Voigt function was used for fitting XRD peak profile analysis. Crystallite size and lattice strain were calculated by using the Williamson–Hall method after deducting the instrumental broadening of the standard sample from peak profile. The milled powder was characterized by scanning electron microscopy (SEM) (FEI Quanta 200 F) operating at 20 kV and transmission electron microscopy (TECNAI G^2 T20) TEM operated at 200 kV. Thermal analysis of 30 h milled powder was performed using differential scanning calorimetry (DSC) of NETZSCH STA 449 F3 apparatus in an argon atmosphere at a heating rate of 10 K/min. In situ XRD was done by using Rigaku Smart Lab (45 kV-200 mA). While doing so, at every set of temperature, the sample was held for at least 10 min to avoid any thermal inhomogeneity. Heat treatments of the powder samples were done in a controlled atmosphere of vacuum-sealed quartz tube to avoid the oxidation. Finally, attempts have been made to consolidate the powder through conventional sintering. In this aspect, the green pellets were prepared using steel die of 10 mm diameter with 49 kN normal load at room temperature using the 30-ton capacity hydraulic press. The microhardness of the sintered pellets was measured through Vickers microhardness tester.

3 Results

Figure 1a displays the X-ray diffraction pattern of equiatomic AlCrFeCoNiZn high-entropy alloy with milling time. At the initial milling (10 min), diffraction peaks corresponding to every constituent elements could be identified. As the milling proceeds for 5 h, intensity of most of the peaks got reduced. It was noticed that few of the peaks corresponding to Co (100) and Zn (100) and (101) lost their identity completely. It means that the dissolution of Co and Zn into the host lattice took place. On further increase in milling for next 5 h, it was found that the first peak of the Al (111) lost its signals. Along with this, additional peaks of Co (101) and Zn (002) (102) (103) lost their identity after 10 h of milling. With the progress of milling for another 5 h, it was noticed that the formation of the solid solution started with structure close to the BCC structure. The formation of the single-phase BCC structure (a = 2.87 ± 0.02 Å) was observed after 20 h of milling. Although, after 20 h MA, the alloy formed the simple solid

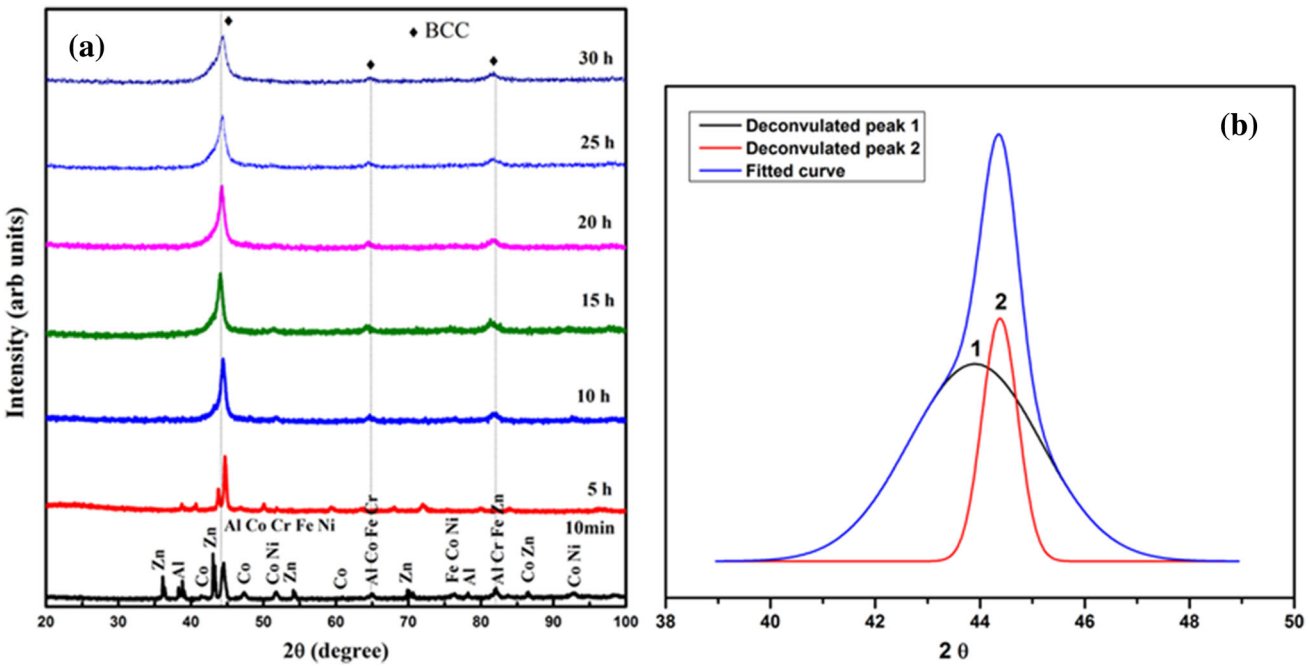

Fig. 1 **a** X-ray diffraction patterns of AlCrFeCoNiZn HEA powder at different milling durations. The evolution of single-phase BCC structure was observed after 30 h of milling time, **b** deconvolution of the first peak of 30 h milled powder

solution, milling was extended for the next 10 h in order to investigate any further phase transformation. The 30 h milled powder showed no change in phase constituents except the broadening of the peaks. This might have happened due to the introduction of lattice strain during the mechanical working of powder and grain refinement [30, 31]. In addition, an asymmetric nature in the first peak of (110) could be observed. The deconvolution of the peak confirmed the presence of mixed phases in the alloy, but the exact nature of second phase could not be discerned based on one peak analysis (see Fig. 1b). The variation of crystallite size and lattice strain with milling time has been calculated and reported in Table 1. Initially, the decrease in crystallite size was significant with high lattice strain which implied that atoms of different sizes were trying to take the position in the host lattice.

The morphology of the 30 h milled powder was studied through scanning electron microscopy (SEM) (see Fig. 2a). It could be observed that the particles were flaky in nature and varied in the range of 1 to $\sim$ 4 μm. This flaky nature of the particles was due to the heavy deformation involved during the mechanical working of powder indicating a good amount of ductility or formability. The SEM–EDX analysis of the 30 h milled powder suggests that the powder was homogeneous in nature (see Fig. 2b). There was no sign of segregation of any elements.

The nanostructure nature of the 30 h milled powder was confirmed by transmission electron microscopy (TEM). Figure 3a, c shows the bright-field (BF) and corresponding selected area diffraction (SAD) pattern of the 30 h milled powder. Figure 3b shows the central dark-field image of the same area. The large distribution of particles in the nanometre range could be ascertained. The formation of the ring pattern in SAD pattern indicates that the alloy particles were randomly oriented in the alloy matrix. Indexing of the ring pattern confirmed the formation of a solid solution phase with a single-phase BCC crystal structure corroborating the similar results obtained from the X-ray diffraction analysis of the 30 h milled powder.

Thermal stability of 30 h milled powder of AlCrFeCoNiZn HEA was investigated through dynamic DSC, and the corresponding thermogram is given in Fig. 4. The first

Table 1 Variation of crystallite size (nm) and lattice strain (%) of equiatomic AlCrFeCoNiZn high-entropy alloy powder with milling time

Milling time (h)	0 h	5 h	10 h	15 h	20 h	25 h	30 h
Crystallite size (nm)	–	55.6	12	10	9	9	8
Lattice strain (%)	–	0.23	0.86	1.07	1.12	1.51	1.87

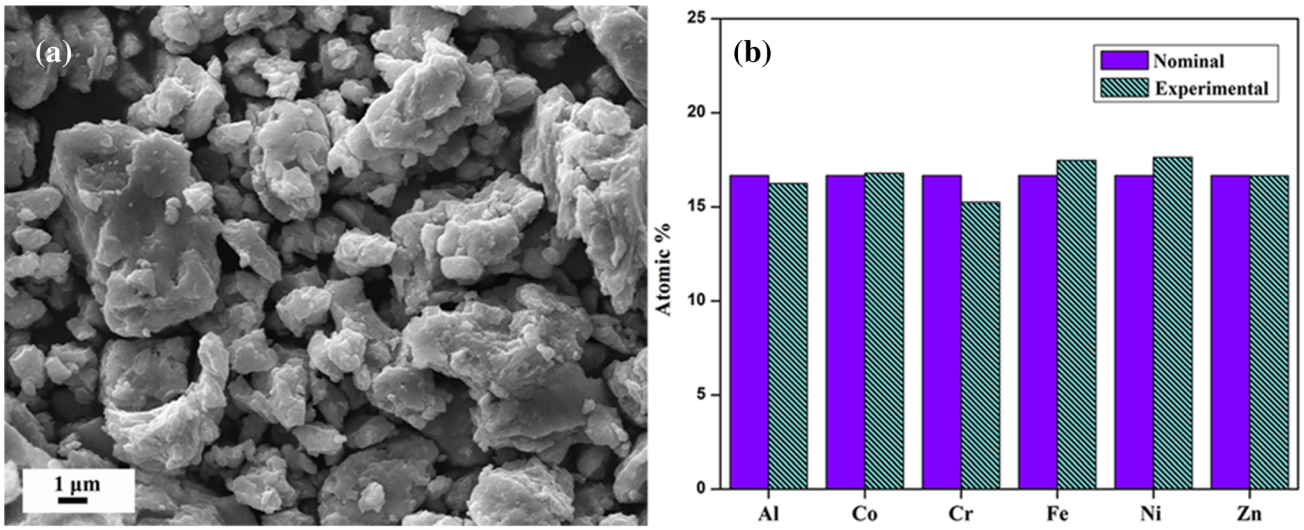

Fig. 2 SEM micrograph of 30 h milled AlCrFeCoNiZn high-entropy alloy. **a** Fractured particles in the range of 1 to ~ 4 µm were observed. **b** Near homogeneous composition of the particles has been confirmed through EDX analysis

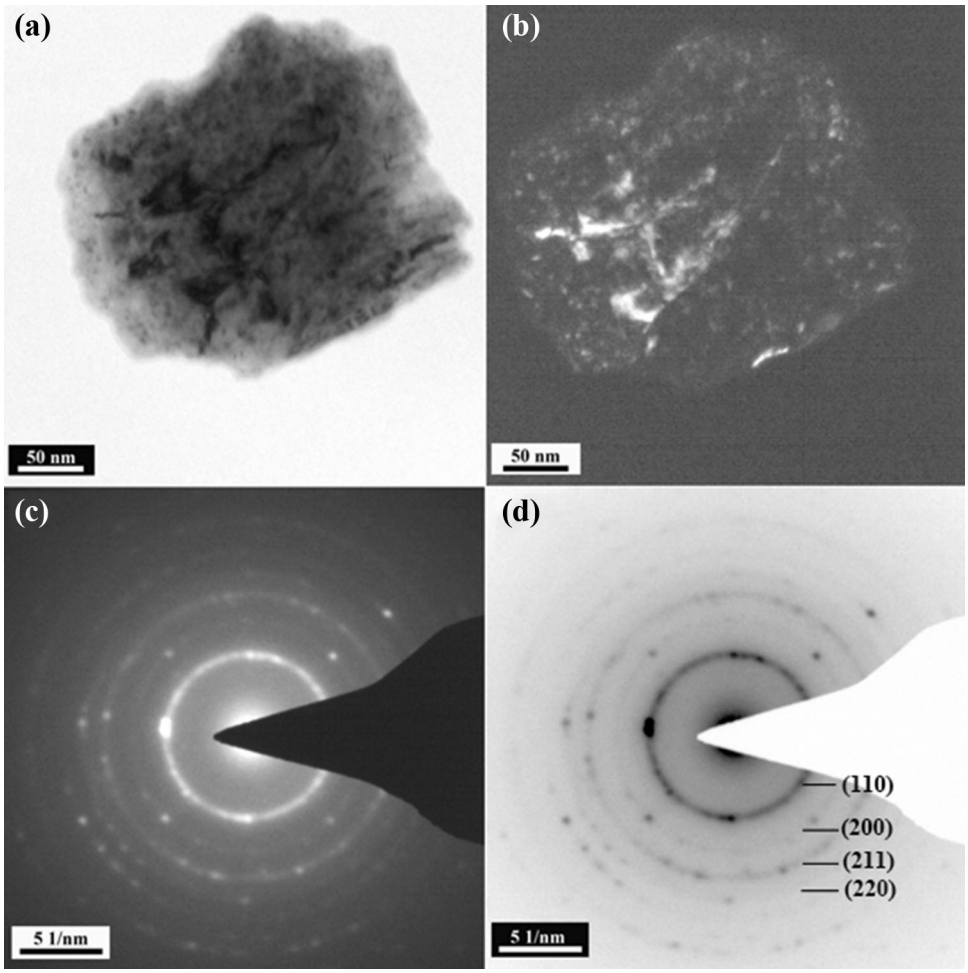

Fig. 3 **a** TEM bright-field image of 30 h milled powder, **b** centre dark-field (CDF) image, **c** corresponding SAD pattern confirms the formation of single-phase BCC structure, **d** inverted image of the same SAD pattern. The nanostructure nature of the milled powder could also be observed

exothermic peak at 323 °C could be believed to be associated with the release of internal stresses arising from structural deformation, lattice strain, etc. The other exothermic peaks (562 °C and 688 °C) were related to the release of energy due to the phase transformation. The shallow nature of endothermic peak (energy absorption) at

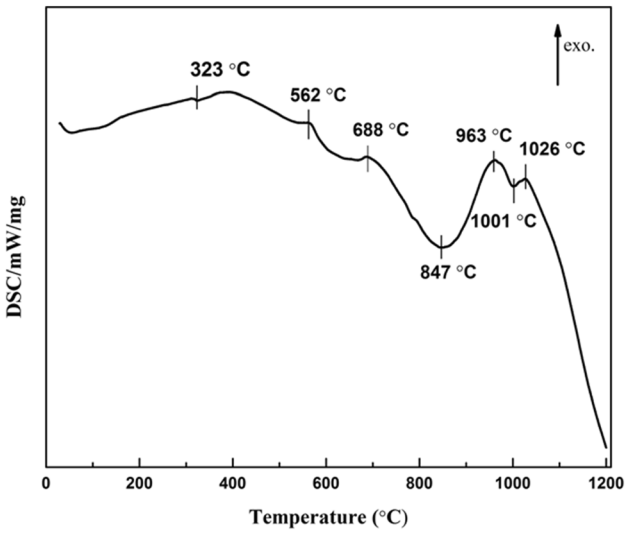

Fig. 4 DSC thermogram of 30 h AlCrFeCoNiZn HEA ball-milled powder

847 °C could also be attributed to phase transformation. The fall of the heating curve after 1026 °C suggests the melting of the alloy. The dynamics of the phase evolution with temperature of AlCrFeCoNiZn HEA was studied through in-situ X-ray diffraction. The multiple displays of the diffraction patterns with temperature (up to 800 °C) are shown in Fig. 5. To avoid any ambiguity in comparison, the diffraction pattern of 30 h milled powder has also been provided in Fig. 5. After careful analysis of every diffraction pattern, no sign of any new phase evolution up to 600 °C was observed. It was further noticed that the broadening of the peaks decreased with the increase in temperature. This happened due to the release of lattice strain involved during the mechanical working of the powder.

The precipitations of new phases were observed at ~ 800 °C. Indexing of the diffraction pattern confirmed that this alloy decomposed into $L1_2$ (a = 3.59 ± 0.02 Å)- and σ (a = 8.81 Å, c = 4.56 Å)-type intermetallic phases. The volume fraction of the $L1_2$ phase appeared to be more compared to the other BCC- and σ-type phase. The exact temperature of stability could not be predicted due to the diffusive nature of phase transformation which involved a range of temperature. Figure 6 shows the X-ray diffraction patterns of the 30 h milled AlCrFeCoNiZn HEA powder heat-treated at 300 and 600 °C for 1 h. These tests were conducted in order to understand the stability of the alloy at a bit longer time. It was observed that this alloy decomposed into a two-phase structure of B2 (ordered BCC)- and $L1_2$ (ordered FCC)-type intermetallic phases even after 300 °C. Similar phases were evolved at a higher temperature of 600 °C. It was noticed that the evolution of the σ-

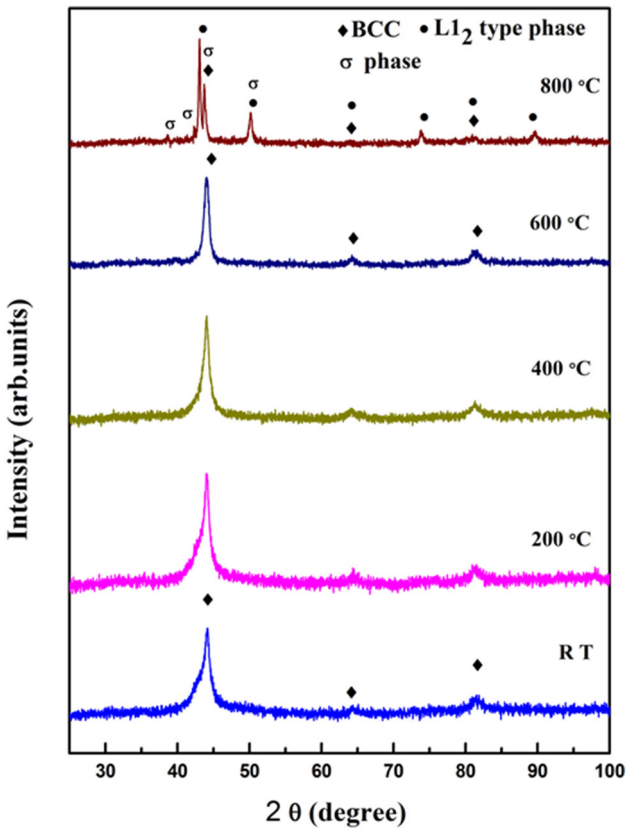

Fig. 5 In situ X-ray diffraction patterns of 30 h milled AlCrFeCoNiZn HEA powder at different temperatures. The precipitation of the $L1_2$- and σ-type intermetallic phases with BCC structure could be observed at ~ 800 °C

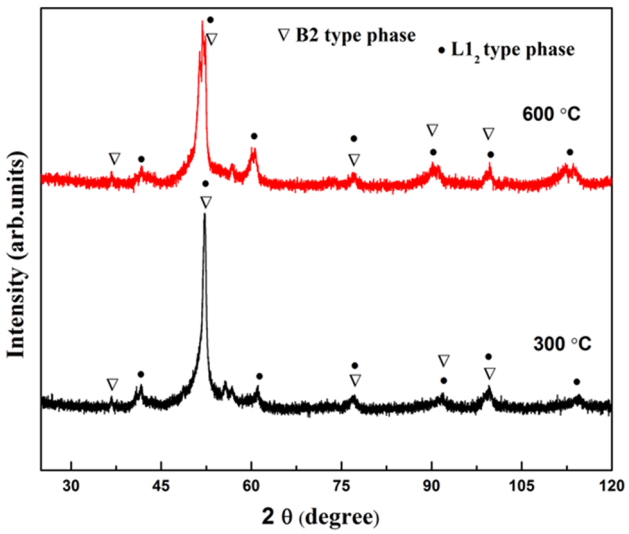

Fig. 6 X-ray diffraction pattern of the 30 h milled powder heat-treated at two temperatures of 300 °C and 600 °C. This heat treatment was done in vacuum quartz tube for 1 h of holding time, evolution of B2- and $L1_2$-type intermetallic phases were observed at both the temperatures

type phase was not observed at these two selected temperatures.

Figure 7 shows the diffraction pattern of the conventionally sintered pellets at 950 °C. The evolution of the B2-, $L1_2$- and σ-type intermetallic phases was observed. The nature of the evolution of the $L1_2$ and σ phases was the same as observed in the in situ diffraction pattern of the 30 h milled powder at 800 °C (Fig. 5). After the consolidation of milled powder, the evolution of the B2 phase was confirmed. So it could be assumed that the B2 phase observed due to the longer holding time of the sintered pellet was similar to that of the heat-treated sample at 300 and 600 °C.

The SEM micrograph and corresponding elemental mapping of the consolidated AlCrFeCoNiZn HEA sintered by pressureless conventional sintering route are given in Fig. 8. In Fig. 8a, two types of grain morphology of grey and white contrast could be observed. This contrast difference occurred due to the two different phases present in the alloy. From SEM elemental mapping, it appeared that white contrast phase was rich in Zn and Cr, grey phase was rich in Ni and Fe and other alloying elements were homogeneously distributed. The distribution of white-type grains was larger in the matrix and varied in the range of 1 to 5 μm. On the other side, grey contrast was evenly distributed with lesser grain size. Theoretical density of the sintered samples was calculated by applying the rule of mixture. The relative density of the samples was calculated by taking the ratio between measured and theoretical densities. It was found that relative density of two samples was 81.5% and 82.2%, respectively. It could be suggested from this study that simultaneous application of pressure and temperature during sintering would lead to better density in the alloy. Microhardness of the sintered samples at 900 °C was measured at 100, 200 and 300 g load, and minimum ten measurements were taken for each sample. No considerable variation of microhardness with load was found. The average microhardness value of these samples was noted to be 340 ± 8 HV. The reason of comparable less hardness to the other compositionally similar HEAs was a result of lower density. Better mechanical properties could be achieved by using advanced sintering technique, i.e. SPS.

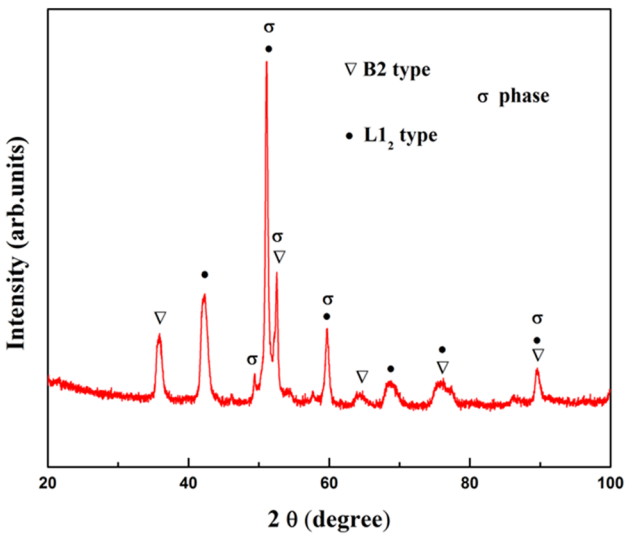

Fig. 7 X-ray diffraction patterns of the sintered pellet at 950 °C. Evolution of B2-, $L1_2$- and σ-type intermetallic phases could be observed

4 Discussion

It has been mentioned in the earlier sections that equiatomic AlCrFeCoNiZn high-entropy alloy is a new member in the HEAs family, as it contains two FCC, two BCC and two HCP elements. Therefore, the phase-forming abilities, the alloying behaviour of these elements with milling time, nature of phase transformation, thermal stability and microstructural evolution after conventional sintering are quite interesting for current alloy. These aspects will be discussed in the following sections.

4.1 Phase-Forming Rules and the Stability of AlCrFeCoNiZn HEA

Phase prediction and their stability is one of the central themes of ongoing research on high-entropy alloys [32]. Earlier studies of HEAs showed that the 'high-entropy' effect (configurational entropy) will stabilize the random solid solution against the intermetallic compounds by adding a large number of alloy elements. The mixing entropy for an equiatomic high-entropy alloy is given by

$$\Delta S_{\text{conf}} = -R\sum_{i=1}^{n}(x_i \ln x_i) \quad (1)$$

where R is the gas constant and x_i the mole fraction of the ith component in the alloy. However, one cannot predict the phase by just calculating the mixing entropy of any particular high-entropy alloy [33]. There are numerous reports of cast HEAs where it has been found that these alloys not only stabilize the solid solution phases but also give rise to a large amount of other phases, i.e. intermetallics and metallic glasses [4]. Therefore, mixing entropy cannot be the only parameter in the design of HEAs [34]. To resolve this complexity, it has been proposed to consider other parameters for formability and stability of high-entropy alloys. In this regard, Zhang et al. [35] have advocated two additional parameters for the design of the HEAs, namely the atomic size difference (δ)

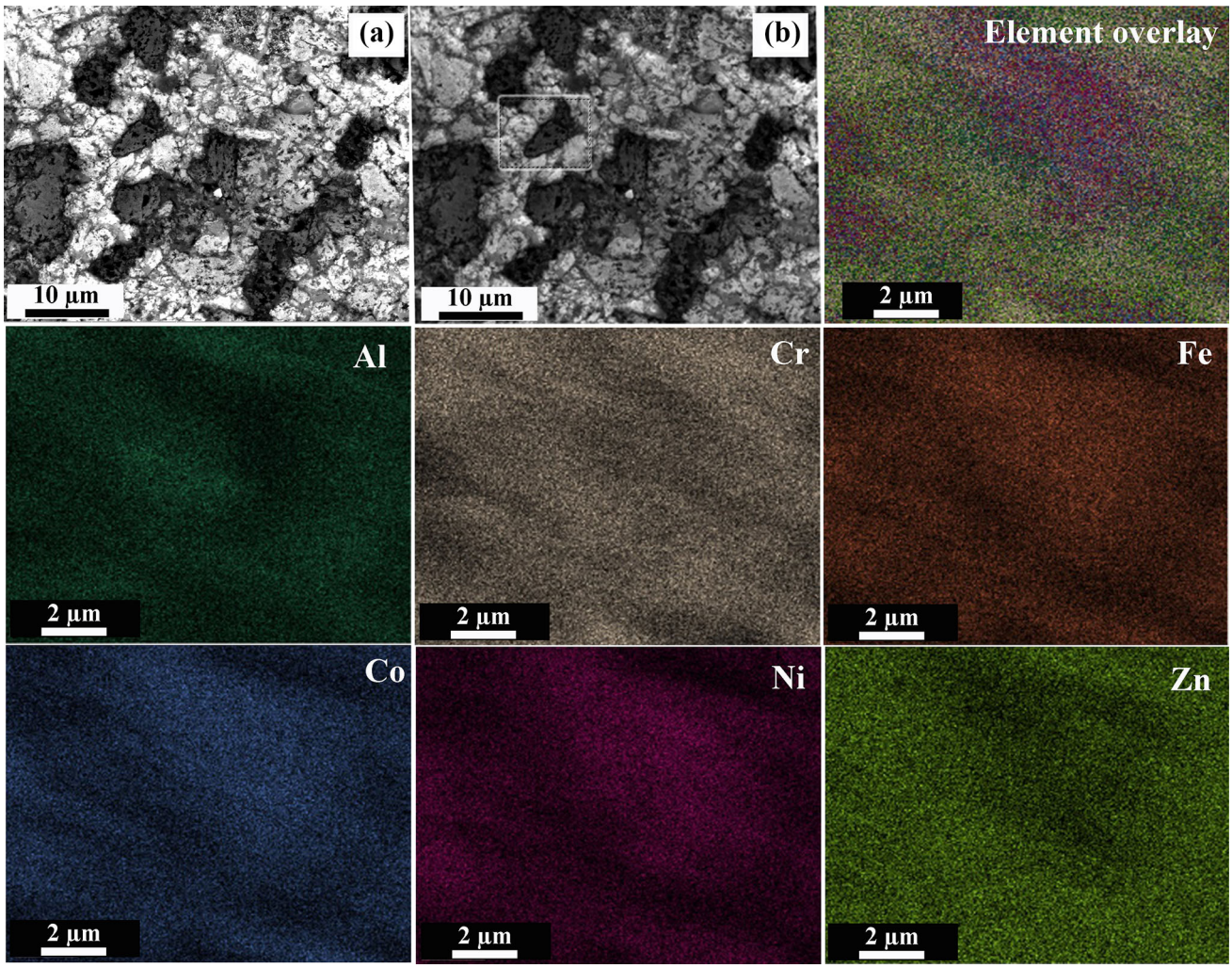

Fig. 8 **a** SEM micrographs of the conventionally sintered pellet at 900 °C. Two types of contrast could be observed from the micrograph. **b** Reference image with marked area for elemental mapping

and mixing enthalpy (ΔH_{mix}). These parameters are described as follows.

$$\delta = 100\sqrt{\sum_{i=1}^{n} c_i\left(1-\frac{r_i}{\bar{r}}\right)^2} \tag{2}$$

where c_i is the concentration of the ith component and $\bar{r}$ is the average value of atomic radii. The calculated value of atomic size difference for current AlCrFeCoNiZn high-entropy alloy is 1.16%. This value fits well within the range of solid solution-forming criteria of $0 \leq \delta \leq 8.5$. Another important parameter known as enthalpy of mixing H_{mix} which can be expressed as:

$$\Delta H_{\text{mix}} = \sum_{i=1, i\neq j}^{n} \Omega_{ij} c_i c_j \tag{3}$$

where $\Omega_{ij} = 4\Delta H_{ij}^{\text{mix}}$ is the regular solution interaction parameter between ith and the jth elements, c_i and c_j are the atomic percentage of the ith and jth component and $\Delta H_{ij}^{\text{mix}}$ is the enthalpy of mixing of the binary equiatomic alloy [36]. The calculated ΔH_{mix} for the current alloy has been found to be − 13.20 kJ/mol, which fits well within the range of $-22 \leq \Delta H_{\text{mix}} \leq 7$ for solid solution formation. The valence electron concentration (VEC) parameter is also the important parameter to be determined for the phase stability of the alloy [37]. VEC is defined as $\text{VEC} = \sum_{i=1}^{n} c_i(\text{VEC})_i$ where $(\text{VEC})_i$ is for the ith element. The calculated value of VEC is evaluated to be 8.00 (Table 2). It has been found that the current alloy does not satisfy the proposed crystal structure (BCC + FCC) based on the VEC value. It is important to point out that Dwivedi et al. [38] have studied the formation of single-phase FCC structure in nanocrystalline CrNbTiVZn HEA by mechanical alloying. The crystal structure of CrNbTiVZn HEA does not conform to the proposed VEC rule. This discrimination has been argued with the non-equilibrium

Table 2 Calculated thermodynamic parameters of AlCrFeCoNiZn high-entropy alloy

Mixing entropy ΔS_{mix} (J/mol-K)	Mixing enthalpy ΔH_{mix} (kJ/mol)	Atomic size difference (%) δ	Valence electron concentration (VEC)
14.89	− 13.20	1.16	8.00

processing route and the ability of the FCC crystal structure to accommodate more atoms than BCC. We would like to mention that these empirical rules are basically derived from the materials that are processed through equilibrium routes. However, in certain conditions, these rules can be extended for the non-equilibrium processing as well for broader sense of understanding of the formation of solid solution phases. In a similar line, Jiang et al. [39] have recently verified the solid solutions rules for single-phase formation and mentioned that these rules can not be strictly applied to all HEAs. Further investigation is required for the applicability of these rules considering the definition of HEAs. Hence, we are of the opinion that these rules are strictly validated for the prediction of solid solution phases and not the exact crystal structure in HEAs.

4.2 Alloying Behaviour and Phase Stability of Nanocrystalline AlCrFeCoNiZn HEA

The alloying behaviour of each element in the equiatomic AlCrFeCoNiZn HEA has been followed systematically with milling. All the reflections of the constituent elements are present after 10 min of milling. Further analysis of the diffraction patterns suggests that Co, Zn and Al start losing their identity, indicating that they are getting dissolved to form solid solution of BCC type. The low melting point of the elements, i.e. Zn and Al can get affected initially due to their higher diffusivity [40]. The complex interaction of the elements may be responsible for the dissolution behaviour of selective elements such as Co.

The dissolution of elements with milling can be schematically represented as follows

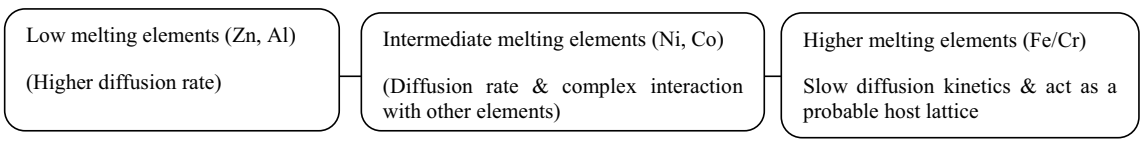

Similar behaviour was observed in our previously reported AlCrFeCoNi and AlCrMnFeCoNi high-entropy alloys. It has been mentioned earlier that this alloy forms a simple solid solution phase of BCC structure even after 20 h of milling, though the milling is extended up to 30 h. The 30 h milled powder shows the single-phase BCC structure with lattice parameter (a) of 2.87 ± 0.02 Å. There is no sign of further phase transformation. From the lattice parameter, it can be predicted that the Fe lattice acts as a host lattice (Fe, a = 2.86 Å) and may not be the Cr lattice as Cr has higher lattice parameter. The lattice parameter of final milled powder is close to that of Fe than Cr. From diffraction patterns of AlCrFeCoNiZn HEA, it has been observed that broadening of the peaks increases with milling time which may be attributed to the reduction in crystallite size and increase in lattice strain with milling time. The variation of crystallite size and lattice strain with milling time is given in Table 1.

4.3 Stability of the Phases During Thermal Treatment of AlCrFeCoNiZn HEA

It has been observed from dynamic DSC thermogram that the alloy shows the diffusive type of phase transformation behaviour as indicated through intermittent endothermic peaks. The shallow peak at ∼ 847 °C is attributed to the major phase transformation. These observations are further supported through in situ XRD (Fig. 4). It has been noticed that there is no new phase evolved up to 600 °C. On further increase in temperature at the higher side (800 °C), the evolution of new phases is detected. These new phases are found to correspond to the $L1_2$ (a = 3.59 ± 0.02 Å) and Cr–Co-based σ (a = 8.81 Å, c = 4.56 Å)-type intermetallics. The formation of the σ phase in all the Cr-containing HEAs is very common and has been reported in the literature. It has been found that Cr promotes the formation of σ phase in the presence of the Fe, Co and Ni. To understand the thermal stability of the alloy, heat treatment of powder samples was done at two different temperatures, i.e. 300 and 600 °C for 1 h in a vacuum-sealed quartz tube. It has been observed that the alloy decomposes into two intermetallic phases such as B2- and $L1_2$-type coexisting with a minor amount of Cr–Fe–Co-based σ phase. These phases can be retained at a higher temperature of 600 °C. So it can be concluded that the alloy is not stable at 300 °C temperature for a higher holding time. This holding time is not sufficient for in situ XRD where it takes time to dissolve into two phases. It means that diffusion kinetics of

Table 3 Calculated binary mixing enthalpy (ΔH_{mix}) of AlCrFeCoNiZn HEA by Miedema approach

Element	Al	Co	Cr	Fe	Ni	Zn
Al	–	− 22	− 12	− 13	− 26	1
Co	− 22	–	− 5	− 2	0	− 14
Cr	− 12	− 5	–	− 2	− 7	− 3
Fe	− 13	− 2	− 2	–	− 2	− 4
Ni	− 26	0	− 7	− 2	–	− 18
Zn	1	− 14	− 3	− 4	− 18	–

phase transformation is perhaps slow in the current AlCrFeCoNiZn high-entropy alloy. Consolidated samples of AlCrFeCoNiZn HEA at 950 °C show the existence of similar phases, i.e. B2-, $L1_2$- and σ-type intermetallics. These phases were also reported in our previous work on AlCrFeCoNi and AlCrMnFeCoNi HEA. Hence it can be concluded that due to the higher mixing entropy of the Al–Ni binary elements, these elements start forming an ordered structure during the heat treatment (Table 3). The formation of σ phase is well reported in alloys close to present composition at higher temperature [41]. The present alloy also falls in the same line of phase evolutions as the previously reported AlCrFeCoNi and AlCrMnFeCoNi HEA except for low thermal stability [25, 26]. However, low melting element Zn perhaps affects the thermal stability of the alloy.

5 Conclusions

The following conclusions can be drawn from the present investigation:

1. A newly designed composition of 30 h milled equiatomic AlCrFeCoNiZn leads to the formation of a simple solid solution phase of BCC ($a = 2.87 \pm 0.02$Å) crystal structure closely adopting the structure of Fe.
2. The alloy is not thermally stable, and after heat treatment, it has transformed to the B2-, $L1_2$- and σ-type intermetallic phases. Sintered pellet at 950 °C also shows the evolution of similar intermetallic phases.
3. The formation of B2-, $L1_2$- and σ-type intermetallic phases is very common in the Al-, Co-, Cr-, Fe- and Ni-containing high-entropy alloys. It has been confirmed from the study of AlCrFeCoNiZn, that Zn has affected neither the evolution of phases nor the structure of the milled product. However, it has lowered the stability of the milled BCC phase.
4. The present alloy satisfies the prescribed range of the semi-empirical thermodynamic parameters for forming a solid solution in the as-milled HEAs. However, in the heat-treated condition, it leads to the formation of three phases deviating from the HEAs, but possibly leading to the medium entropy alloys.

Acknowledgements The authors would like to thank Dr. Joysurya Basu, Dr. Manish Kumar Singh, Mr. Vivek Kumar Pandey and Mr. Yagnesh Shadangi for many useful discussions during the course of this investigation.

References

1. Ranganathan S, *Curr Sci* **85** (2003) 1404.
2. Yeh J W, Chen S K, Lin S J, Gan J Y, Chin T S, Shun T T, Tsau C H, and Chang S Y, *Adv Eng Mater* **6** (2004) 299.
3. Cantor B, Chang I T H, Knight P, and Vincent A J B, *Mater Sci Eng A* **375–377** (2004) 213.
4. Ye Y F, Wang Q, Lu J, Liu C T, and Yang Y, *Mater Today* **19** (2016) 349.
5. Mukhopadhyay N K, *Curr Sci* **109** (2015) 665.
6. Tsai M H, and Yeh J W, *Mater Res Lett* **2** (2014) 107.
7. Otto F, Yang Y, Bei H, and George E P, *Acta Mater* **61** (2013) 2628.
8. Wang Y P, Li B S, and Fu H Z, *Adv Eng Mater* **11** (2009) 641.
9. Yao M J, Pradeep K G, Tasan C C, and Raabe D, *Scr Mater* **72–73** (2014) 5.
10. Yadav T P, Mukhopadhyay S, Mishra S S, Mukhopadhyay N K, and Srivastava O N, *Philos Mag Lett* **97** (2017) 494.
11. Pickering E J, and Jones N G, *Int Mater Rev* **61** (2016) 183.
12. Senkov O N, and Miracle D B, *J Alloys Compd* **658** (2016) 603.
13. Sharma A S, Yadav S, Biswas K, and Basu B, *Mater Sci Eng* R **131** (2018) 1.
14. Zhang K B, Fu Z Y, Zhang J Y, Wang W M, Wang H, Wang Y C, Zhang Q J, and Shi J, *Mater Sci Eng A* **508** (2009) 214.
15. Bhadeshia H K D H, *Mater Sci Technol* **31** (2015) 1139.
16. Shivam V, Shadangi Y, Basu J, and Mukhopadhyay N K, *J Mater Res* **35** (2019) 787.
17. Zhang Y, Ting T, Tang Z, Gao M C, Dahmen K A, Liaw P K, and Ping Z, *Prog Mater Sci* **61** (2014) 1.
18. Koch C C, *Mater Res Lett* **32** (2017) 3435.
19. Varalakshmi S, Kamaraj M, and Murty B S, *J Alloys Compd* **460** (2008) 253.
20. Suryanarayana C, *Prog Mater Sci* **46** (2001) 1.

21. Raviathul Basariya M, Srivastava V C, and Mukhopadhyay N K, *Mater Des* **64** (2014) 542.
22. Shadangi Y, Shivam V, Singh M K, Chattopadhyay K, Basu J, and Mukhopadhyay N K, *J Alloys Compd* **797** (2019) 1280.
23. Varalakshmi S, Kamaraj M, and Murty B S, *Metall Mater Trans A Phys Metall Mater Sci* **41** (2010) 2703.
24. Vaidya M, Prasad A, Parakh A, and Murty B S, *Mater Des* **126** (2017) 37.
25. Shivam V, Basu J, Pandey V K, Shadangi Y, and Mukhopadhyay N K, *Adv Powder Technol* **29** (2018) 2221.
26. Shivam V, Basu J, Shadangi Y, Singh M K, and Mukhopadhyay N K, *J Alloys Compd* **757** (2018) 87.
27. Thurston K V S, Gludovatz B, Hohenwarter A, Laplanche G, George E P, and Ritchie R O, *Intermetallics* **88** (2017) 65.
28. Borkar T, Gwalani B, Choudhuri D, Mikler C V, Yannetta C J, Chen X, Ramanujan R V, Styles M J, Gibson M A, and Banerjee R, *Acta Mater* **116** (2016) 63.
29. Praveen S, Murty B S, and Kottada R S, *Mater Sci Eng A* **534** (2012) 83.
30. Suryanarayana C, Ivanov E, and Boldyrev V, *Mater Sci Eng A* **304** (2001) 151.
31. Basariya M R, Srivastava V C, and Mukhopadhyay N K, *Philos Mag* **96** (2016) 2445.
32. Miracle D B, and Senkov O N, *Acta Mater* **122** (2017) 448.
33. Guo S, Hu Q, Ng C, and Liu C T, *Intermetallics* **41** (2013) 96.
34. Yang X, and Zhang Y, *Mater Chem Phys* **132** (2012) 233.
35. Zhang Y, Zhou Y J, Lin J P, Chen G L, and Liaw P K, *Adv Eng Mater* **10** (2008) 534.
36. Miedema A R, de Châtel P F, and de Boer F R *Phys B* **100** (1980) 1.
37. Guo S, and Liu C T, *Prog Nat Sci Mater Int* **21** (2011) 433.
38. Dwivedi A, Koch C C, and Rajulapati K V, *Mater Lett* **183** (2016) 44.
39. Jiang L I, *JOM*, (2020).
40. Chen Y L, Hu Y H, Hsieh C A, Yeh J W, and Chen S K, J Alloys Compd **481** (2009) 768.
41. Mohanty S, Maity T N, Mukhopadhyay S, Sarkar S, Gurao N P, Bhowmick S, and Biswas K, *Mater Sci Eng A* **679** (2017) 299.